Inorganic Chemistry

Article

pubs.acs.org/IC

Synthesis and Structural Characterization of Group 4 Metal Carboxylates for Nanowire Production

Timothy J. Boyle,* Daniel T. Yonemoto, Thu Q. Doan, and Todd M. Alam

Advanced Materials Laboratory, Sandia National Laboratories, 1001 University Boulevard, SE, Albuquerque, New Mexico 87106, United States

Supporting Information

ABSTRACT: The synthesis and characterization of a series of group 4 carboxylate derivatives ($[M(ORc)_4]$ where M = Ti, Zr, Hf) was undertaken for potential utility as precursors to ceramic nanowires. The attempted syntheses of the $[M(ORc)_4]$ precursors were undertaken from the reaction of $[M(OBu^t)_4]$ with a select set of carboxylic acids (H-ORc where ORc = OPc ($O_2CCH(CH_3)_2$), OBc ($O_2CC(CH_3)_3$), ONc ($O_2CCH_2C(CH_3)_3$)). The products were identified by single-crystal X-ray diffraction studies as $[Ti(\eta^2\text{-}OBc)_3(OBu^t)]$ (**1**), $[Zr_2(\mu_3\text{-}O)(\mu\text{-}OPc)_4(\mu,\eta^2\text{-}OPc)(\eta^2\text{-}OPc)]_2$ (**2**), $[H]_2[Zr(\eta^2\text{-}OBc)_2(OBc)_2(OBc)_2]$ (**3**), $[Zr(\mu\text{-}ONc)_2(\eta^2\text{-}ONc)_2]_2$ (**4**), or $[Hf(\mu\text{-}ORc)_2(\eta^2\text{-}ORc)_2]_2$ [ORc = OPc (**5**), OBc (**6**, shown), ONc (**7**)]. The majority of compounds (**4**–**7**) were isolated as dinuclear species with a dodecahedral-like (*CN*-8) bonding mode around the metals due to chelation and bridging of the ORc ligand. The two monomers (**1** and **3**) were found to adopt a capped trigonal prismatic and *CN*-8 geometry, respectively, due to chelating ORc and terminal ORc or OBu^t ligands. The metals of the oxo-species **2** were isolated in octahedral and *CN*-8 arrangements. These compounds were then processed by electrospinning methods (applied voltage 10 kV, flow rate 30–60 μL/min, electric field 0.5 kV/cm), and wire-like morphologies were isolated using compounds **4**, **6** (shown), and **7**.

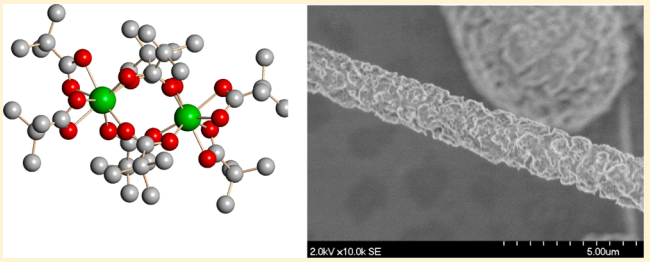

INTRODUCTION

Group 4 ceramic oxide materials have found widespread applicability ranging from paints to cosmetics to thermal barrier coatings to computer memories to high dielectric constant materials to integrated circuits to refractory materials, to name just a few. Due to their commercial availability, air stability, and solubility in water, frequently used precursors for the production of these oxide materials are metal carboxylates ($[M(ORc)_x]$).[1−3] A search of the crystallographic literature indicates that there are no homoleptic group 4 derivatives[4] available (only carboxy, oxides),[4−14] and therefore it is not surprising that these are not commercially available.

The production of high aspect ratio nanowires of MO_2 (M = Ti, Zr, Hf) was undertaken due to their high dielectric constant (*k*) nanowires. Nanowires are of interest since the micrometer dimension (length) supplies a means to connect these materials to the "real world" while maintaining the unusual properties associated with the nanodimension (width). While numerous routes to ceramic nanowires have been reported (i.e., mechanochemical,[15] seeded growth off of a liquid-phase chemical approach,[16] ice particulates as porogen material,[17] hydrothermal,[18,19] laser ablation,[19] anodization,[19] and many more), these are typically a result of complicated chemistries developed under protracted studies that often do not necessarily translate to other systems. One way to overcome the chemistry variables presented in the different nanowire systems (*vide infra*) is to use a processing route that can generate wires without the complicated preparation or processing.

The emphasis of this study focused on exploiting electrospinning (ES) processing[20−24] since it offers a simple and continuous methodology for the production of high aspect ratio fibers (widths are nanometers with lengths ranging from nano- to micrometers). Typically, ES methodologies employ polymers to ensure chain entanglement occurs, thereby generating a solution with high levels of molecular cohesion. This addition results in an increase in the surface tension of the drop, preventing Plateau−Rayleigh instability, ensuring a charged liquid jet expulsion (ES) occurs versus electrospraying of droplets.

Our interest was to develop precursors that will circumvent the need to use polymers in ES methods to minimize postprocessing. Previously, we demonstrated that ES of $[Sn(\mu\text{-}NR_2)(OR)]_2$ and $[Sn(OR)_2]$ precursors dissolved in THF successfully led to the isolation of either Sn^0 or SnO nanowires, without the use of a polymer.[25] As our research on directly ES nanoceramic materials continued, the production of high *k* group 4 ceramic materials came to the forefront. From the early ES results on a variety of these precursors, it became apparent that a "linker" would be needed to ensure wire formation occurred. Carboxylate (ORc) ligands were selected

Received: August 4, 2014
Published: November 17, 2014

   dx.doi.org/10.1021/ic501904m | *Inorg. Chem.* 2014, 53, 12449−12458

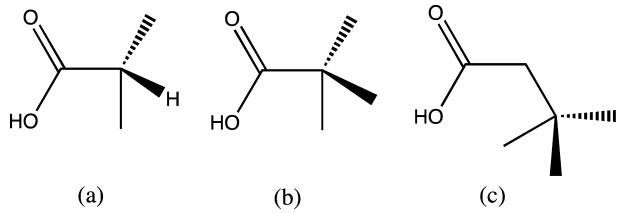

Figure 1. Schematic representation of the carboxylic acids (H-ORc) used: (a) isobutyric acid (H-OPc), (b) trimethylacetic acid (H-OBc), and (c) *tert*-butylacetic acid (H-ONc).

based on their propensity to act as a bridge between metals[4] and structural tunability based on variations in the steric bulk of the pendant chain: isobutyric acid ($HO_2CCH(CH_3)_2$ or H-OPc), trimethylacetic acid (HOBc or $H\text{-}O_2CC(CH_3)_3$), and *tert*-butylacetic acid (H-ONc, $H\text{-}O_2CCH_2C(CH_3)_3$); see Figure 1a–c, respectively. Using this series of HORc a family of modified $M(OR)_4$ precursors ($[M(ORc)_n(OR)_{4-n}]$ n = 1–4) were developed in addition to our previously reported species[26,27] and used for the investigation of ES processing for production of MO_2 (M = Ti, Zr, Hf) nanowires.

While we have synthesized this family of $[M(ORc)_n(OR)_{4-n}]$, for this report, only the *attempts* at fully substituted products will be presented. The products isolated from the reaction conditions noted for eq 1 were identified by single-crystal X-ray diffraction studies as $[Ti(\eta^2\text{-}OBc)_3(OBu^t)]$ (**1**), $[Zr_2(\mu_3\text{-}O)(\mu\text{-}OPc)_4(\mu,\eta^2\text{-}OPc)(\eta^2\text{-}OPc)]_2$ (**2**), $[H]_2[Zr(\eta^2\text{-}OBc)_2(OBc)_2(OBc)_2]$ (**3**), $[Zr(\mu\text{-}ONc)_2(\eta^2\text{-}ONc)_2]_2$ (**4**), or $[Hf(\mu\text{-}ORc)_2(\eta^2\text{-}ORc)_2]_2$ [ORc = OPc (**5**), OBc (**6**), ONc (**7**)]. The [H] in front of the structure is used to indicate the necessary but not located hydrogen in the crystal structure. Additional analytical data confirmed the bulk material was consistent with these structures. These compounds were preliminarily explored as precursors for ES production of ceramic nanowires. The details of the precursors' synthesis and characterization and ES ceramic materials generated are described.

$$[M(OBu^t)_4] + 4\ \text{H-ORc} \xrightarrow{\text{solv}} [M(ORc)_4]_n + 4\ \text{H-OBu}^t$$
$$\text{M = Ti, Zr, Hf;}\quad \text{ORc = OPc, OBc, ONc} \tag{1}$$

EXPERIMENTAL SECTION

All compounds described below were handled with rigorous exclusion of air and water using standard Schlenk line and glovebox techniques unless otherwise discussed. All solvents and precursors were used as received (from Aldrich and Alfa Aesar) without further purification, including toluene, THF, H-OPc, H-OBc, H-ONc, and $[M(OBu^t)_4]$ (M = Ti, Zr, Hf). Dried crystalline materials were used for all analytical analyses.

FTIR data were collected on a Nicolet 6700 FTIR spectrometer using a KBr pellet press under a flowing atmosphere of nitrogen. Elemental analyses were collected on a PerkinElmer 2400 Series II CHNS/O analyzer, with samples prepared in an argon-filled glovebox. Thermogravimetric analysis (TGA) data were collected on a Mettler Toledo TGA/DSC 1 STAR^e System instrument at 5 °C/min ramp rate under a flowing argon atmosphere to 650 °C. All NMR samples were prepared using crystalline material handled under an argon atmosphere, at a fixed concentration. Spectra were collected on a Bruker Avance-III 500 NMR spectrometer under standard experimental conditions: ^{1}H analysis was performed with a 4 s recycle delay at 16 scans; chemical shifts were referenced to the chloroform-*d* peak at 7.24 ppm. The ^{1}H PFG NMR diffusion experiments used a stimulated echo (STE) sequence with bipolar gradient pulses and a spoil gradient pulse, a fixed gradient pulse length of δ = 1 ms, using the interpulse delay of Δ = 250–300 ms, and 16 gradient steps between 1 and 54 G/cm. The gradient strength was calibrated using the self-diffusion coefficient (D) of water at 298 K (2.3×10^{-9} m^2/s). The echo decay $E(q, \Delta)$ was fit using the standard Stejskal–Tanner formula,[28] where D is the experimentally measured self-diffusion coefficient (m^2 s^{-1}), Δ is the diffusion period, and $q = \gamma\delta g/2\pi$, which is the product of the gyromagnetic ratio of the observed nuclei (γ), the gradient strength (g), and the length of the gradient pulse (δ) (see eq 2).

$$\frac{E(q, \Delta)}{E(0, \Delta)} = \exp\left[-q^2 D\left(\Delta - \frac{\delta}{3}\right)\right] \tag{2}$$

As a first approximation the diffusion of a spherical molecule can be described by the Sutherland–Einstein relation shown in eq 3.

$$D = \frac{k_B T}{6\pi\eta R} \tag{3}$$

where η is the viscosity and R is the hydrodynamic radius of the molecule. To provide an estimate of differences in complex size (i.e., volume), we have taken the ratio of the D for the cluster with respect to the THF solvent molecules using eq 4.

$$\frac{D_{\text{cluster}}}{D_{\text{THF}}} \approx \frac{R_{\text{THF}}}{R_{\text{cluster}}} \tag{4}$$

This disregards any shape factor corrections for different aggregate shapes possible in the analysis.

General Reaction. In an inert atmosphere glovebox, 4 equiv of the desired HORc was added to a clear solution of the desired $[M(OBu^t)_4]$ dissolved in ~5 mL of toluene. After stirring for 12 h, the clear solution was then set aside with the cap loose to allow the volatile component of the reaction to evaporate. Upon crystallization, the mother liquor was decanted and some crystals were set aside for X-ray analysis. The remaining crystals were dried *in vacuo*, and the resulting white powders were used without further purification. Yields were not optimized but instead reflect the first batch isolated.

*$[Ti(\eta^2\text{-}OBc)_3(OBu^t)]$ (**1**).* $Ti(OBu^t)_4$ (1.00 g, 2.94 mmol), H-OBc (1.20 g, 11.8 mmol), and 5 mL of toluene. Yield: 59.2% (0.74 g). FTIR (KBr, ν_{max}/cm^{-1}): 2977(s), 2930(m, sh), 2905(m, sh), 2873(m,sh), 1655(m), 1648(m), 1560(s), 1484(s), 1459(m), 1419(s), 1377(m), 1362(m), 1228(s), 1183(w), 1027(s), 724(s), 607(m), 581(m), 571(m), 448(m). ^{1}H NMR (500.1 MHz, tol-d_8): δ 1.32 (9H, s, $OC(CH_3)_3$ 1.19 (28H, s, $O_2C(CH_3)_3$). Anal. Found: C, 53.70; H, 8.91. Calcd for $C_{19}H_{36}O_7Ti$: C, 53.78; H, 8.55.

*$[Zr_2(\mu_3\text{-}O)(\mu\text{-}OPc)_4(\mu,\eta^2\text{-}OPc)(\eta^2\text{-}OPc)]_2$ (**2**).* $Zr(OBu^t)_4$ (1.00 g, 2.60 mmol), H-OPc (0.92 g, 10.4 mmol), and 5 mL of toluene. Yield: 64.6% (0.62 g). FTIR (KBr, ν_{max}/cm^{-1}): 2972(s), 2932(m), 2872(w), 1655(w,sh), 1601(s), 1560(s,sh), 1534(s,sh), 1511(s,sh), 1476(s), 1434(s), 1378(m), 1363(m), 1299(m), 1170(w), 1098(m), 934(m), 861(m), 777(w), 661(m), 568(m), 540(m). ^{1}H NMR (500.1 MHz, tol-d_8): δ 2.48 (0.9H, s(br), $OCH(CH_3)_2$), 1.09 (6H, d, $O_2CH(CH_3)_2$, J_{H-H} = 6.3 Hz). Anal. Found: C, 41.33; H, 6.18. Calcd for $C_{102}H_{174}O_{52}Zr_8$: C, 41.36; H, 5.92.

*$[H]_2[Zr(\eta^2\text{-}OBc)_2(OBc)_2(OBc)_2]$ (**3**).* $Zr(OBu^t)_4$ (0.50 g, 1.30 mmol), H-OBc (0.53 g, 5.21 mmol), and 5 mL of toluene. Yield: 54.9% (0.50 g). FTIR (KBr, ν_{max}/cm^{-1}): 2965(s), 2931(m), 2871(w), 1626(s), 1596(s), 1546(m), 1509(s,sh), 1496(s), 1430(s), 1381(m), 1364(m), 1230(s), 1175(w), 1032(w), 938(w), 910(m), 816(w), 787(w), 642(w), 607(s), 529(w), 505(w), 436(m). ^{1}H NMR (500.1 MHz, $CDCl_3$): δ 1.18 (6H, s, $O_2CC(CH_3)_3$). Anal. Found: C, 51.15; H, 8.32. Calcd for $C_{30}H_{56}O_{12}Zr$: C, 51.47; H, 8.08.

*$[Zr(\mu\text{-}ONc)_2(\eta^2\text{-}ONc)_2]_2$ (**4**).* $Zr(OBu^t)_4$ (0.50 g, 1.30 mmol), H-ONc (0.60 g, 5.2 mmol), and 5 mL of toluene. Yield: 63.3% (0.50 g). FTIR (KBr, ν_{max}/cm^{-1}): 2956(s), 2907(m), 2870(m), 1719(w), 1708(w), 1650(m,sh), 1630(s), 1597(m), 1560(m), 1523(m), 1478-(s,sh), 1460(s), 1417(s), 1367(m), 1304(w), 1276(w), 1232(m), 1199(w), 1149(w), 1047(w), 969(w), 935(w), 912(w), 812(w),

dx.doi.org/10.1021/ic501904m | *Inorg. Chem.* 2014, 53, 12449–12458

Table 1. Data Collection Parameters for 1−7

	1	1a	2	3	4
chemical formula	$C_{19}H_{36}O_7Ti$	$C_{38}H_{72}O_{15}Ti_2$	$C_{48}H_{84}O_{26}Zr_4$	$C_{30}H_{54}O_{12}Zr$	$C_{48}H_{88}O_{16}Zr_2$
fw	424.351	864.75	1442.03	697.95	1103.63
temp (K)	173	173	173	173	173
space group	orthorhombic *pmn*21	monoclinic *P*21/*c*	monoclinic *P*21/*n*	orthorhombic *Pbca*	triclinic $P\bar{1}$
a (Å)	15.9892(11)	22.8500(14)	13.0666(4)	11.3570(8)	11.8579(13)
b (Å)	8.1331(6)	11.2011(8)	12.2893(3)	19.3700(13	14.5616(17)
c (Å)	9.2864(5)	19.0227(13)	19.4521(5)	35.211(2)	22.069(3)
α (deg)					72.483(2)
β (deg)		94.305(4)	91.102(2)		78.790(2)
γ (deg)					68.688(1)
V (Å^3)	1207.62(14)	4855.0(6)	3123.03(15)	7745.9(9)	3369.9(7)
Z	2	4	2	8	2
D_{calcd} (Mg/m^3)	1.167	1.183	1.533	1.197	1.088
μ(Mo K*α*) (mm^{-1})	0.386	0.386	0.726	0.334	0.360
R1[a] (%) (all data)	6.17 (12.42)	7.10 (9.62)	3.44 (4.91)	6.00 (9.45)	5.14 (8.46)
wR2[b] (%) (all data)	14.38 (18.92)	20.00(23.19)	11.29 (13.16)	16.55 (19.45)	13.62 (15.43)

	5	6	6a	7
chemical formula	$C_{32}H_{56}Hf_2O_{16}$	$C_{40}H_{60}Hf_2O_{16}$	$C_{60}O_{26}Hf_4$	$C_{96}H_{176}Hf_4O_{32}$
fw	1053.75	1153.86	1851.57	2556.33
temp (K)	173	173	173	173
space group	monoclinic *Cc*	monoclinic *P*2(1)/*c*	triclinic $P\bar{1}$	triclinic $P\bar{1}$
a (Å)	13.9141(4)	16.148(5)	14.328(2)	11.3388(5)
b (Å)	14.3507(4)	20.579(6)	15.095(3)	11.8903(6)
c (Å)	20.4389(6)	21.896(7)	22.532	43.709(2)
α (deg)			95.2330(19)	86.329(2)
β (deg)	94.170(1)	110.520(2)	104.0970(19)	86.672(2)
γ (deg)			116.6680(17)	87.272(2)
V (Å^3)	4070.4(2)	6815(4)	4109.1	5865.2(5)
Z	4	4	2	4
D_{calcd} (Mg/m^3)	1.720	1.135	1.167	1.447
μ(Mo K*α*) (mm^{-1})	5.161	3.089	5.098	3.596
R1[a] (%) (all data)	2.06 (2.15)	6.15 (14.14)	15.01 (17.48)	8.37 (9.66)
wR2[b] (%) (all data)	5.39(6.67)	13.43 (16.39)	39.52 (42.62)	25.91 (26.70)

[a] $R1 = \sum||F_o| - |F_c||/\sum|F_o| \times 100$. [b] $wR2 = [\sum w(F_o^2 - F_c^2)^2/\sum(w|F_o|^2)^2]^{1/2} \times 100$.

808(w), 757(m), 726(w), 633(w), 583(w,sh), 528(w), 447(w). ^{1}H NMR (500.1 MHz, $CDCl_3$): *δ* 2.18 (2H, s, $O_2CCH(C(CH_3)_3)$), 1.01 (9.5H, s, $O_2CCH(C(CH_3)_3)$). Anal. Found: C, 53.14; H, 8.54. Calcd for $C_{54}H_{100}O_{18}Zr_2$: C, 53.17; H, 8.26.

[Hf(μ-OPc)$_2$(η^2-OPc)$_2$]$_2$ (**5**). Hf(OBu^t)$_4$ (0.50 g, 1.06 mmol), H-OPc (0.37 g, 4.25 mmol), and 5 mL of toluene. Yield: 85.7% (0.48 g). FTIR (KBr, ν_{max}/cm^{-1}): 2972(s), 2931(m), 2873(w), 1702(w), 1546(s), 1478(s), 1438(s), 1379(m), 1364(m), 1300(s), 1232(w), 1099(s), 936(m), 863(m), 778(w), 663(w), 540(w). ^{1}H NMR (500.1 MHz, tol-d_8): *δ* 2.55 (2H, s(br), $O_2CH(CH_3)_2$), 1.16 (6H, s(br), $O_2CH(CH_3)_2$), 1.01 (6H, s(br), J_{H-H} = 4.9 Hz, $O_2CH(CH_3)_2$). Anal. Found: C, 36.85; H, 5.58. Calcd for $C_{16}H_{28}HfO_8$: C, 36.47; H, 5.36.

[Hf(μ-OBc)$_2$(η^2-OBc)$_2$]$_2$ (**6**). Hf(OBu^t)$_4$ (0.50 g, 1.06 mmol), H-OBc (0.43 g, 4.25 mmol), and 5 mL of toluene. Yield: 93.55% (0.58 g). FTIR (KBr, ν_{max}/cm^{-1}): 2966(m), 2931(m), 2872(w), 1736(w), 1702(m), 1633(s), 1602(m), 1550(s), 1509(s,sh), 1488(s), 1436(s), 1384(m), 1365(s), 1231(s), 1032(w), 940(w), 913(s), 818(m), 794(m), 610(m), 574(w), 429(w). ^{1}H NMR (500.1 MHz, tol-d_8): *δ* 1.09 (1.0H, s, $O_2C(CH_3)_3$). Anal. Found: C, 40.86; H, 6.41. Calcd for $C_{20}H_{36}HfO_8$: C, 41.20; H, 6.22.

[Hf(μ-ONc)$_2$(η^2-ONc)$_2$]$_2$ (**7**). Hf(OBu^t)$_4$ (0.50 g, 1.06 mmol), H-ONc (0.49 g, 4.25 mmol), and 5 mL of toluene. Yield: 73.5% (0.50 g). FTIR (KBr, ν_{max}/cm^{-1}): 2956(m), 2907(m), 2870(m), 1645(s), 1597(s), 1560(s), 1533(s), 1457(s, br), 1418(s), 1366(s), 1306(m), 1277(m), 1234(m), 1198(s), 1150(m), 1037(s), 990(w), 970(w), 935(w), 913(m), 803(m), 789(w), 758(m), 727(m), 635(m), 579(w), 531(w), 444(w). ^{1}H NMR (500.1 MHz, tol-d_8): *δ* 2.29 (2H, s, $O_2CH_2C(CH_3)_3$), 0.99 (9H, s, $O_2CHC(CH_3)_3$). Anal. Found: C, 43.17; H, 6.85. Calcd for $C_{24}H_{44}HfO_8$: C, 45.10; H, 6.94.

General X-ray Crystal Structure Information. Single crystals were mounted onto a loop from a pool of Fluorolube and immediately placed in a cold N_2 vapor stream, on a Bruker AXS diffractometer employing an incident-beam graphite monochromator, Mo K*α* radiation (*λ* = 0.710 70 Å), and a SMART APEX CCD detector. Lattice determination and data collection were carried out using SMART version 5.054 software. Data reduction was performed using SAINTPLUS version 6.01 software and corrected for absorption using the SADABS program within the SAINT software package. Structures were solved by direct methods or by using the Patterson method, which yielded the heavy atoms, along with a number of the lighter atoms. Subsequent Fourier syntheses yielded the remaining light-atom positions. The hydrogen atoms were fixed in positions of ideal geometry and refined using SHELX software. The final refinement of each compound included anisotropic thermal parameters for all non-hydrogen atoms. All final CIF files were checked using the CheckCIF program (http://www.iucr.org/). Additional information concerning the data collection and final structural solutions can be found in the Supporting Information or by accessing CIF files through the Cambridge Crystallographic Data Base. Table 1 lists the unit cell parameters for the structurally characterized compounds **1**−**7**.

Specific issues for problematic structures are presented below. The slightly higher *R*-values associated with **1** and **7** are due to disorder in the *tert*-butyl moieties. For **4** a volume equivalent to 659.5 Å (equivalent to a HONc molecule) and for **6** a volume of 3074.8 Å (estimated to be approximately equivalent to 3 molecules of toluene)

dx.doi.org/10.1021/ic501904m | *Inorg. Chem.* 2014, 53, 12449−12458

were squeezed out using the Platon squeeze method. EADP was used to model (50/50) disorder: **5** on C(19) with C(20), C(11) w/C(12); **7** on C(4) w/C(3), C(56) w/C(50), C(58) w/C(59), C(4) w/C(12), C(5) w/C(46), C(6) w/C(48), C(60) w/C(53), and C(2) w/C(8). Significant disorder was noted for the Bu^t group containing C(29) but was successfully modeled.

Viscosity Measurements. The viscosities of the 0.66 M sample solutions generated using **5**−**7** were measured. In a standard setup, a cone and plate rheometer (Thermo Haake RheoStress 300, Germany) with a 1° cone angle and a 60 mm diameter, maintained at 25 °C with a recirculating temperature bath, was used. Shear rate sweeps were performed from 100 to 700 s^{-1} over 2 min, held at a shear rate of 700 for 15 s, then decreased to 100 s^{-1} again over 2 min to determine if hysteresis was present in any sample. The rising and falling shear rate data exhibited good overlap and little hysteresis, indicative of dissolved precursor solutions in the solvent.

Electrospinning Synthesis. An experimental setup, as previously described, was used to evaluate **1**−**7** for direct production of ceramic nanowires.[25] In short, under a nitrogen atmosphere, a 66 mM precursor/THF solution was transferred to a horizontally fixed syringe pump (model MD-1000, Bioanalytical Systems Inc.). An electrode connected to a high-voltage power supply (model DEL HVPS INST 230 30KV, Spellman High Voltage Electronics Corporation) was attached to the tip of the metallic needle. The ES process to produce the ceramic nanowires was carried out using the stock solution under the following conditions: flow rate (FR) was 30−60 μL/min; 10 kV, electric field (EF) was 0.5 kV/cm. The charge was applied and ES was performed for ∼60 min.

RESULTS AND DISCUSSION

In order to directly electrospin high dielectric constant group 4 oxide ceramic nanowires, it was thought that highly soluble precursors with ligands that could "link" the ES drops together would be of the most interest. It was anticipated that this would require lower nuclearity complexes that possessed terminal ORc ligands. A search of [M(ORc)$_4$] precursors, omitting less desirable ligands for ES of ceramic oxide materials (i.e., halide, cyclopentadienyl, hydroxide, and oxalate ligands), yields only a handful of crystallographically characterized homometallic species.[5−14] The majority of these ORcs are based on the methacrylato derivative,[5−9] and all are large oligomers that possess an oxo ligand.[4] Moraru et al. also reported on some large oligomers of heterometallic group 4 OMc derivatives.[29] Due to this surprising void, we undertook the synthesis of a series of [M(ORc)$_n$(OR)$_{4-n}$] compounds following eq 1. For this report only the results for the synthesis and characterization of the *attempts* (eq 1, n = 4) at homoleptic species are discussed, followed by the initial foray into their utility as ES precursors.

Synthesis. Upon mixing of the HORc with the [M(OR)$_4$] of interest in toluene, the solutions remained clear without the formation of a precipitate. After stirring for 12 h, crystals were isolated by slow evaporation of the volatile component, samples removed for single-crystal X-ray diffraction studies (Table 1), and the remainder of the crystals dried and used for all further investigations. The analytical data for these compounds are discussed below, by cation: (A) titanium (**1**); (B) zirconium (**2**−**4**); and (C) hafnium (**5**−**7**). A discussion of the ES processing results of these compounds follows. For the two oxo species isolated (**1a** and **6a**) in the preparation of this report, the unit cell parameters have been reported in Table 1, with more information available in the Supporting Information.

A. Titanium Derivatives. For the Ti/ORc system, only the OBc derivative yielded crystalline material with the OPc and ONc derivatives isolated as oils. For **1**, the FTIR data revealed no OH stretch but did display OBc carbonyl bends and stretches (1655, 1648, 1560 cm^{-1}) that were significantly varied from the free H-OBc (1710 cm^{-1}) spectrum. ^{1}H NMR data indicated two singlets in a 1:3 ratio, which was initially interpreted as a dimer with one bridging and three terminal OBc ligands ([Ti(μ-OBc)(OBc)$_3$]$_2$). In order to understand the structural properties better, a single-crystal X-ray structure was obtained. The structure of **1** (Figure 2) proved to be a

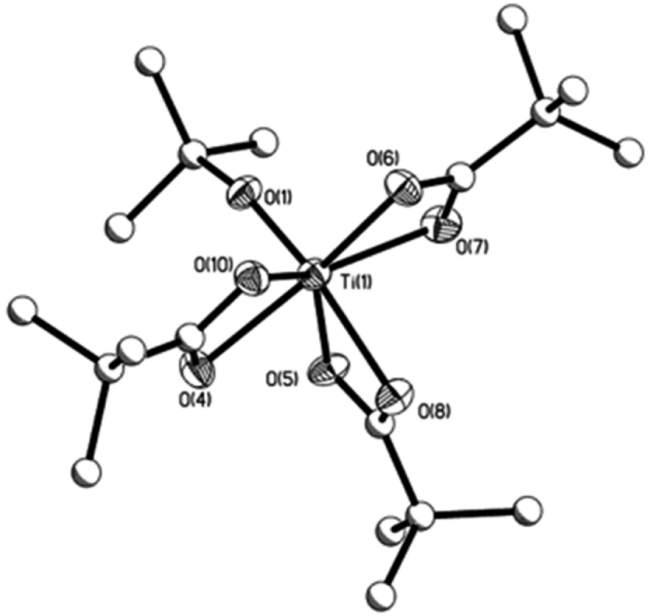

Figure 2. Structure plot of **1**. Thermal ellipsoids are drawn at the 30% level. Hydrogen atoms have been removed for clarity.

monomeric seven-coordinated complex with three chelating OBc ligands and one terminal OBu^t. The proton ratio is 1:3 (OBu^t:OBc), which explains the NMR spectrum. The elemental analyses of the bulk powder were found to be in agreement with the observed structure of **1**. The full substituted species could not be isolated, which was attributed to the small cation size and the significant steric bulk of the ligands.

There are only a few compounds with a Ti that is seven- or higher-coordinated by O atoms. Of this group of compounds, removing heterometallic species, solvated water, calixarene, or salt derivatives leaves only a few potential model compounds. Since the ethanediolato[30] or catecholato[31] derivatives were not reasonable examples for a metrical comparison, the carbamate species ([Ti(O$_2$C-NR$_2$)$_4$[c]]) *N*,*N*-alkylcarbamato (R = Me,[32] Et,[33] Pr^i[34]) were selected. These complexes had Ti−O distances (av 2.07 Å) that were found to be in line with those noted for **1** (2.08 Å); see Table 2. The O−Ti−O (av 61.4°) and O−C−O (av 118.3°) angles of **1** were also similar to the carbamato[33,34] derivatives [O−Ti−O (av 62.7°) and O−C−O (av 115.8°)]. The Ti−OBu^t distance of **1**, 1.702 Å, is the shortest reported for any crystallographically characterized O$_3$Ti−OBu^t (1.736[35]−1.862[36] Å) moiety that has been disseminated in the database.[4] Exposure of **1** to air led to the formation of an oxo complex with the general formula [(μ-O)[Ti(μ-OBc)(OBc)$_2$(OBu^t)]$_2$] (**1a**). Details of the structure and the characterization of the complex are available in the Supporting Information.

To further assist in distinguishing the precursor solution properties, pulse field gradient (PFG) diffusion NMR experi-

dx.doi.org/10.1021/ic501904m | Inorg. Chem. 2014, 53, 12449−12458

Table 2. Average Metrical Data for 1−7

	metal						
	Ti	Zr			Hf		
distances (Å)	**1**	**2**	**3**	**4**	**5**	**6**	**7**
M−OBu^t	1.72						
M−O		2.07(μ_3)					
M---M		3.36−3.38		4.24	4.24	4.23	4.23
M(ORc)			2.13				
M(η^2-ORc)	2.09	2.26	2.24	2.23	2.22	2.22	2.22
M(μ,η^2-ORc)		2.41(μ) 2.28					
M(μ-ORc)		2.18		2.16	2.14	2.13	2.14
angles (deg)	**1**	**2**	**3**	**4**	**5**	**6**	**7**
ORc−M−O$_{unique}$ (cis)	99.1	80.4	83.7	77.0	80.4	78.8	80.0
(trans)	158.7	151.5	154.3	150.1	150.0	150.5	150.1
O^c−M−O^c	62.0	56.0	57.8	59.1	57.4	57.7	58.3
(μ,η^2)O−C−O		117.8					
O−C−O			123.1				
η^2(O−C−O)	116.6	117.3	118.1	117.6	115.8	116.4	116.6
μ-(O−C−O)		124.8		123.2	124.6	123.1	123.3
M−O−M		107.3 to 134.9					

Table 3. Summary of Properties of 1−7

cmpd	nucl	ES morph	mp (°C)	TGA (wt % loss)	max sol THF (M)	viscosity 66 mM ES solution (cP)	PFG NMR[a] THF-d_8 $D \times 10^{-10}$ (m^2/s) (% composition)	estim'd volume[b] (THF) (Å^3)	relative volume[c] (THF)
1	1	absent	47/65	80.0	0.50		13 (99%) 0.01 (1%)	512	1
2	4	spray	180	50.0	0.05		10.0	1125	2.2
3	1	spray	109	56.5	0.80		8.6	1768	3.4
4	2	wire-like	91	65.0	0.77		7.6	2563	5.0
5	2	dots	56	58.0	0.15	0.561	9.3	1398	2.7
6	2	wires	55	62.5	0.06	0.568	9.9	1149	2.2
7	2	wires	54/85	27.5	0.44	0.622	11.5	740	1.4

[a]Two diffusion constants (i.e., mixture of the two sizes listed). [b]Estimated (spherical) volume based on scaling with respect to THF, its diffusion constant, and a volume of 72 Å^3. [c]Relative volume = [(estimated volume)/(estimated volume of **1** (512))].

ments were attempted. No special sample preparation was required except that each sample was run in the same solvent at the same concentration and temperature. Samples of **1** prepared in toluene-d_8 or $CDCl_3$ were found to yield one compound in solution based on a single self-diffusion rate (D). Upon dissolution in the Lewis basic solvent THF-d_8, the D for **1** in THF-d_8 revealed two values (see Table 3), indicative of two species present. The minor species was present at 1% and may be explained by some minor amount of acid or solvent present.

B. Zirconium Derivatives. The Zr derivatives were also synthesized according to eq 1 (n = 4), under similar conditions noted for the Ti system. Using Zr(OBu^t)$_4$ no significant change in the clear, colorless solution upon addition of the HORc modifiers was noted. After stirring for 12 h, with no apparent change in the reaction mixture, the volatile component was removed *in vacuo*, yielding a white powder. Again, the lack of the −OH (3200 cm^{-1}) stretch and the ingrowth of the ORc stretches and bends proved to be a useful metric for determining that the reaction had proceeded to completion. The main carbonyl stretch of the H-ORc (1780 cm^{-1} HOPc, 1710 cm^{-1} HOBc, 1780 H-ONc cm^{-1}) shifted slightly with an increased number of stretches (OPc, 1601, 1476, 1434 cm^{-1}; OBc, 1596, 1486, 1430 cm^{-1}; ONc, 1630, 1460 cm^{-1}). Solution ^{1}H NMR indicated that symmetric molecules were present in solution with only one set of broad resonances consistent with the particular, pendant ORc chain of **2**−**4** being observed. Since these data did not facilitate a structural understanding, single-crystal X-ray studies were undertaken to assist in elucidating their molecular arrangement.

The OPc derivative could be isolated only as the oxo species **2** and is shown in Figure 3. For this cluster, a standard Zr$_4$(μ_3-O)$_2$ core was solved with a center of symmetry relating the two halves. Each half of the molecule consists of two eight-coordinated Zr atoms bound by oxygen atoms of the OPc. Zr(1) uses two μ-OPc ligands to bridge to Zr(2) and two more to bridge to Zr(2A). It completes its coordination sphere by chelating one OPc and using an oxygen from a μ,η^2-OPc from Zr(2). The coordination sphere of Zr(2) is filled by four μ-OPc ligands, two μ_3-O atoms, and one μ,η^2-OPc ligand that bridges back to Zr(1). This moiety has a mirror plane of symmetry that forms the tetranuclear species **2**. Additional structural representations are available in the Supporting Information.

The structure of OBc derivative **3** (Figure 4) proved to be monomeric using four terminal OBc ligands and two chelating OBc ligands in a *trans* arrangement. Due to charge balance, two protons are necessary but could not be located in the final structure and have been added externally to represent their

dx.doi.org/10.1021/ic501904m | *Inorg. Chem.* 2014, 53, 12449−12458

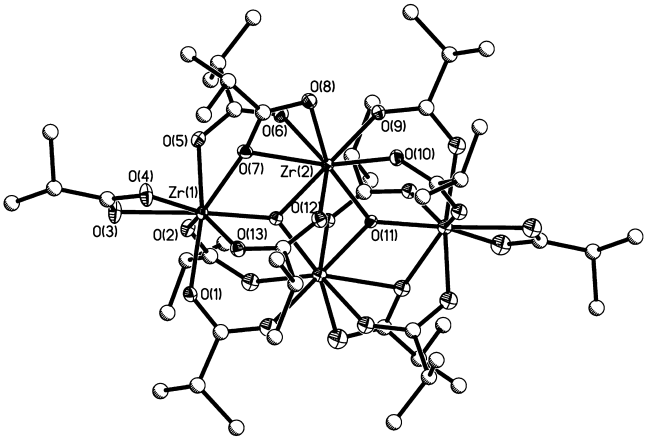

Figure 3. Structure plot of **2**. Thermal ellipsoids are drawn at the 30% level. Hydrogen atoms have been removed for clarity.

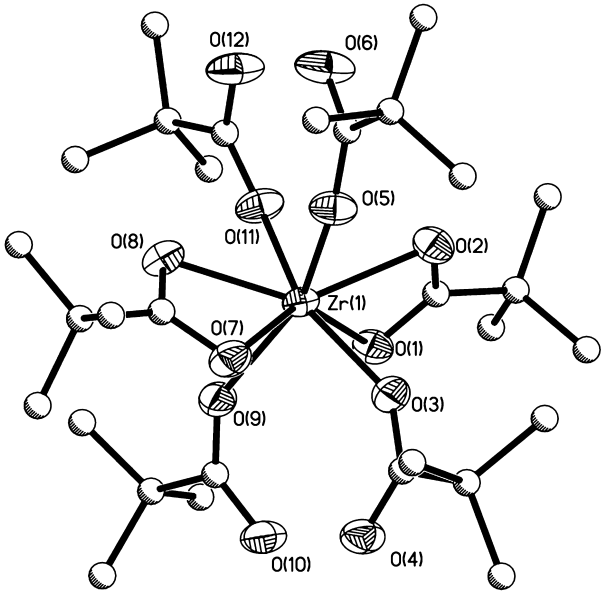

Figure 4. Structure plot of **3**. Thermal ellipsoids are drawn at the 30% level. Hydrogen atoms have been removed for clarity.

presence. This leaves the Zr in an eight-coordinate oxygen environment, which is not uncommon for Zr compounds;[4] however, the homo-ORc monomer is unique among reported carboxylate derivatives of Zr.[4]

Adding a methylene group to the chain (i.e., using the ONc ligand) led to another homocarboxylate derivative, but compound **4** was found to be the dinuclear complex shown in Figure 5. The increase in nuclearity from **3** to **4** was attributed to the steric bulk of the Bu^t group being removed by the addition of the methylene linkage in the ONc pendant chain (Figure 1). Each Zr is eight-coordinated by oxygens from the ORc ligands with four bridging and two terminal chelating ONc ligands. These chelating ONc ligands are *cis* to each other in this case. Again, no similar structure types are presently available for comparison to **4**.[4]

Of the more than 160 structures reported for a Zr-ORc system, only 68 of these compounds possess an O−C−O moiety acting as the source of the oxygen atoms around the metal center; however, none of the structures reported to date represent homocarboxylate derivatives. There are a number of carboxylate oxo species[6,8,9,12,14] that will have to suffice as

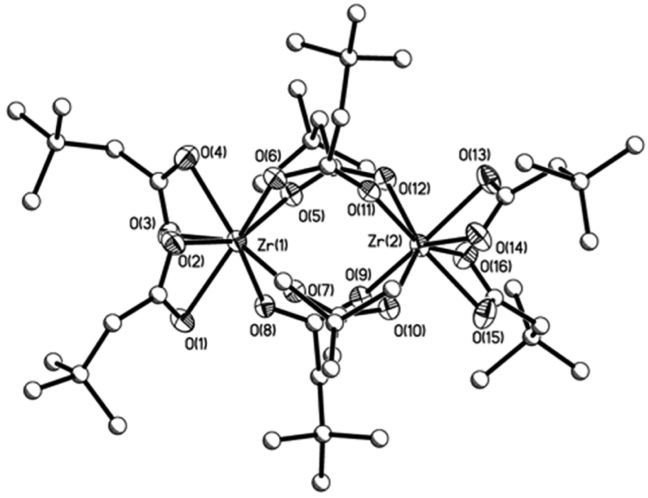

Figure 5. Structure plot of **4**. Thermal ellipsoids are drawn at the 30% level. Hydrogen atoms have been removed for clarity.

molecular models for metrical comparisons including $[Zr_4(O)_4(methacrylate)_{12}]$[8] and $[Zr_4(O)_2(methacrylate)_{12}]$ (and the C_6H_6 solvate).[6] The chelating O−Zr−O and O−C−O angles of these compounds were found to be 57.3° and 118.2° with the bridging μ-(O−C−O) angles av 124.3°.[6,8] In comparison, the metrical data for **2**−**4** [av O−Zr−O = 57.6°; O−C−O = 117.5°; μ-(O−C−O) = 124.0°] were found to be in-line with these data (see Table 2). Further, the bond distance and angles of **2**−**4** are consistent with each other.

The elemental analyses of the bulk powders proved to be consistent with the single-crystal structures for **3** and **4**. For **2**, a half of a molecule of toluene per molecule of **2** led to an acceptable analysis; therefore, the bulk powders were considered to be consistent with the solid-state structures. On the basis of the established purity, the ^{1}H NMR spectra were re-evaluated. The data presented indicate either the molecule has been disrupted or dynamic exchange is occurring between the bridging and chelating ligands. Variable-temperature NMR (VT-NMR) spectroscopic studies could not be undertaken to determine the solution behavior due to preferential crystallization. Dilution of the sample did not yield a significant change in the spectra, which indicates no equilibrium was occurring. PFG NMR diffusion analyses were undertaken, and only one species was found to be present in THF-d_8 solutions for **2**−**4** (see Table 3). Therefore, it was reasoned that in THF-d_8 dynamic exchange of the ligands was occurring.

C. Hafnium Derivatives. Switching to Hf was not expected to impact the reaction product structure due to the similarity in cation size and charge with Zr.[37] The FTIR spectra of the Hf derivatives revealed a loss of the OH peak stretch and similar carboxylate shifts (OPc, 1546, 1478, 1438 cm^{-1}; OBc, 1633, 1488, 1436 cm^{-1}; ONc, 1645, 1457 cm^{-1}) as noted for the Zr analogues. The ^{1}H NMR data were again simple single sets of resonances, except for the OPc product, which displayed two types of OPc methyl doublets at low concentration, which is consistent with the observed structure of **5** (Figure 6). At higher concentration, the same peaks were noted but were observed as broad singlets. In general, this indicated that the Hf structures would be analogous to that noted for **2**−**4**.

Not surprising, the structures of **5**−**7** (Figures 6−8, respectively) were found to be similar to each other and that

dx.doi.org/10.1021/ic501904m | *Inorg. Chem.* 2014, 53, 12449−12458

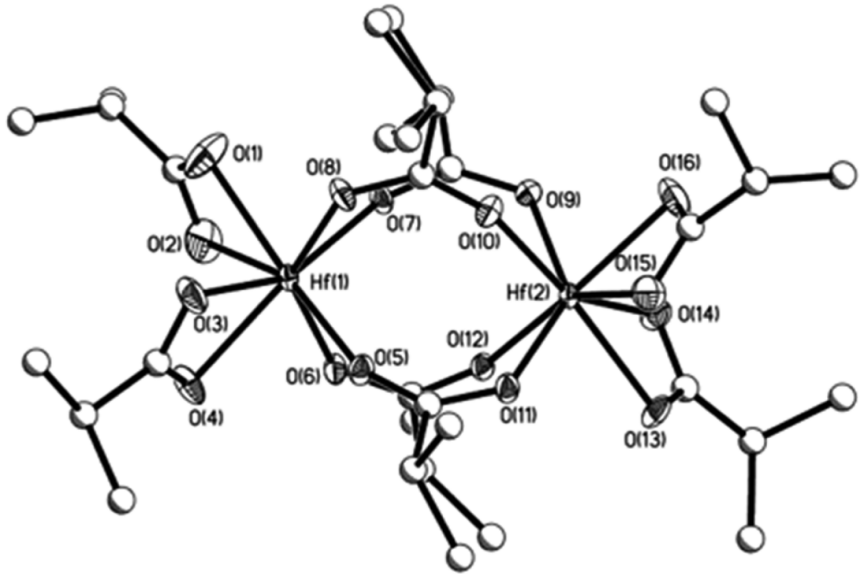

Figure 6. Structure plot of **5**. Thermal ellipsoids are drawn at the 30% level. Hydrogen atoms have been removed for clarity.

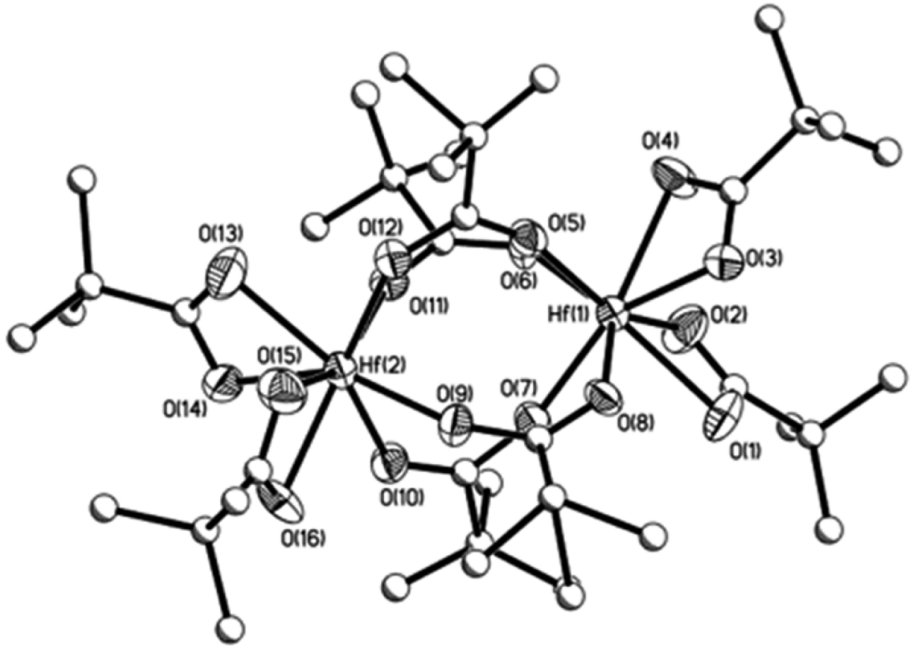

Figure 7. Structure plot of **6** with thermal ellipsoids drawn at the 30% level. Hydrogen atoms have been removed for clarity.

of **4** (with the Zr replaced by a Hf center). The Hf structures **5**−**7** consist of two terminal chelating ORc and four bridging ORc ligands, forming eight-coordinated Hf metal centers.

Of the 25 species identified with some form of O−C−O moiety acting as the source of the oxygen atoms (4 or more) around the Hf metal center, none of the structures reported to date represent homocarboxylate derivatives. The $[Hf_4(O)_2(\text{methacrylate})_{12}]$[5] and the $[Hf_{12}(OAc)_6(OAc)_{18}(\mu_3\text{-}O)_8(\mu_3\text{-}OH)_8]$ (OAc = acetate)[38] are the only reasonable model systems. The Hf−ORc distances of these compounds range from 2.14 to 2.29 Å with O−C−O and chelating O−Hf−O angles that range from 114.5° to 127.3° and 56.1° to 57.6°, respectively. In comparison, those distances and angles noted for **5**−**7** fall within this range. Another oxo species was also observed from an extended growth effort of the Hf/OBc system as $[Hf_2(\mu_3\text{-}O)(\mu\text{-}OBc)_4(\mu_c\text{-}OBc)(\eta^2\text{-}OBc)]_2$ (**6a**, Figure 6b). While the central core was unequivocally identified as being consistent with **2**, the quality of the structure is not acceptable to discuss due to significant disorder in the ligands. Structural data parameters for **6** can be found in Table 1, with additional information available in the Supporting Information.

The elemental analyses of these compounds were in line with the solid-state structure for **5** and **6**. For the ONc derivative **7**, loss of a *neo*-pentyl moiety allows for an acceptable analysis, which is not unexpected, as it has been previously noted.[26] On the basis of the good agreement of the elemental analyses, it was not surprising that the PFG NMR diffusion analyses found only one species in solution for **5**−**7** (THF-d_8).

With these results, the PFG NMR diffusion data of **1**−**7** could be reviewed to elucidate their solution behavior. Compound **1** was expected to retain a monomeric species in solution, and that initial effective volume (D) was used as the

dx.doi.org/10.1021/ic501904m | *Inorg. Chem.* 2014, 53, 12449−12458

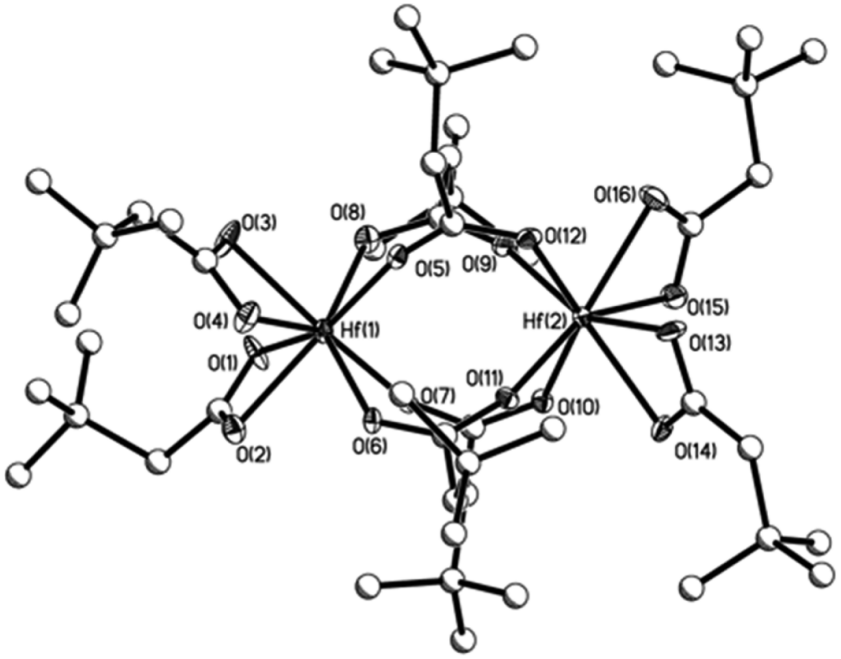

Figure 8. Structure plot of **7**. Thermal ellipsoids are drawn at the 30% level. Hydrogen atoms have been removed for clarity. Two molecules were solved in the unit cell, but only one is shown for clarity.

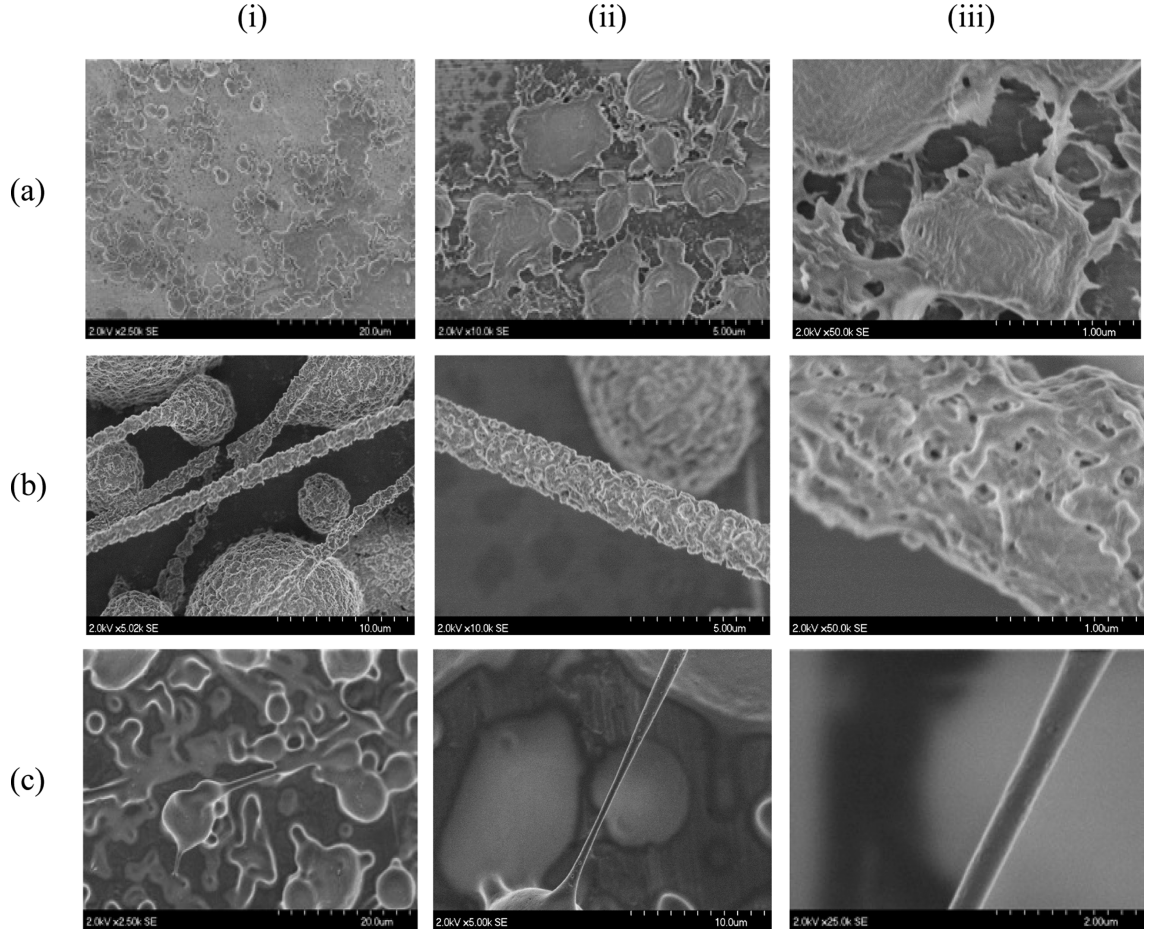

Figure 9. SEM images of materials produced using (a) **5** ES: 10 kV 60 μL/min (scale bar: i = 20 μm, ii = 5 μm, iii = 1 μm), (b) **6** ES: 10 kV, 30 μL/min (scale bar: i = 100 μm, ii = 5 μm, iii = 1 μm), and (c) **7** ES: at 10 kV, 30 μL/min from a 66 mM solution (scale bar: i = 20 μm, ii = 10 μm, iii = 5 μm).

dx.doi.org/10.1021/ic501904m | *Inorg. Chem.* 2014, 53, 12449−12458

baseline to calculate relative volumes (see Table 3). From these calculations it can be reasoned that **7** is also monomeric in solution, whereas, **2**, **3**, **5**, and **6** appear to be larger and assigned to dinuclear complexes. This implies that **3** forms a dinuclear species in solution instead of maintaining its monomeric species, which is not necessarily unreasonable. Either compound **4** adopts a larger cluster than the solid-state structure, or the tumbling in solution makes it appear slightly larger. Since the latter makes more sense, we assume compound **4** retains its structure in solution.

Thermal Analysis. Thermal analyses of **1**−**7** were undertaken to elucidate their utility in conversion to ceramic oxide materials. Using TGA/DSC (see Table 3 and Supporting Information) data, a three-step weight loss for most of the compounds was observed, which was complete by 500 °C for each sample. The weight loss for a number of these precursors (**1**, **5**, **6**) was in-line with expected values (see Table 3); however, none of the Zr adducts (**2**, **3**, **4**) nor the ONc Hf species **7** yielded weight decomposition profiles consistent with the calculated weight losses for complete conversion to the oxide. For the Zr species, the significantly reduced weight loss may be a sign of incomplete combustion. This is possibly due to very stable cores, which are often noted for Zr dinuclear species. The Hf species **7** is the only derivative to show an increase in weight prior to the first weight loss step. This may be a sign of water or oxygen absorption, which would lead to a significant variation in the final weight loss. However, in general, the samples showed very similar decomposition pathways.

Melting point temperatures (see Table 3) were collected, and the majority of compounds were all found to melt below 100 °C, except for the two Zr derivatives (**2** and **3**). The lowest melting is the monomeric Ti (**1**) followed by the Hf derivatives, **5**−**7**. The Zr complexes (**2**−**4**) were found to be the highest melting species in this family of compounds. Two values are reported for **1** and **7**, as they have two distinct slopes in the melting point determination graph. The thermal stability would therefore follow **1** < **5** ∼ **6** ∼ **7** < **4** < **3** < **2** or in general as Ti < Hf < Zr derivatives. The stability of a compound is governed by several factors, but the major influence is the M−O interaction. As can be seen from Table 2, the M−O distances were solved as Ti > Hf > Zr, which follows the size of the cations (0.75 Å Ti < 0.85 Å Hf < 0.86 Å Zr).[37] The stability of the Zr_2O_2 core is widely reported in the literature,[4,39] and it is not surprising that it has the highest decomposition temperature.

Electrospinning. With this variety of well-characterized carboxylate derivatives in hand, their potential to generate ceramic nanowires directly via ES processing from a THF solution was preliminarily tested. In general, ES works by applying a high electrical field to a drop of precursor solution (i.e., polymer) that is pushed through a needle. As the applied high electrical force overcomes the surface energy, the droplet is stretched until a critical point at which a Taylor cone forms to relieve the stress. The resulting emission of the solution goes through a whipping motion and, when collected, can form mats of fibers that possess a high surface area to mass ratio; however, by varying the collector geometry, alignment of the fibers (uniaxial, biaxial, etc.) can be achieved.[20−24]

Under a nitrogen atmosphere, two sets of materials were independently produced to ensure reproducibility of the final product. The maximum concentration was determined for each precursor, and they are listed in Table 3. There was no discernible pattern in terms of cation, pendant ORc chain, or nuclearity that revealed the variations noted. The 66 mM solutions were selected, as this would allow all the compounds to be dissolved. At this dilute concentration, the viscosities of **5**−**7** in THF (THF viscosity = 0.48 cP) were found to be fairly uniform (see Table 3), ranging from 0.56 to 0.62 cP. The results of the ES of these solutions are discussed below based on the precursor's cation: Ti (**1**), Zr (**2**−**4**), and Hf (**5**−**7**; Figure 9a−c). The resulting morphological results are tabulated in Table 3. Some images are shown in Figure 9, with a full sets of the SEM images available in the Supporting Information.

The SEM images of the post-ES materials obtained using monomeric **1** showed only signs of the aluminum substrate. This indicates that the sample never reached the final electrode. Under similar conditions, compounds **2**−**4** were electrospun, and the TEM images for **2** and **3** were irregular, interconnected splotches of material. There was no indication of nanowires or tadpole shapes for these two precursors. In contrast, for **4**, there is some indication of potential wire formation, but nothing definitive could be claimed. Compound **5** proved to produce similar products to those noted above; however, there was some separation between the agglomerated splotches as well as some preliminary linkage between the dots (Figure 9a).

For the last two samples generated from **6** and **7**, the formation of some wires and tadpole structures (Figure 9b and c, respectively) was observed in the samples. While **6** formed dots, tadpoles, and wires, of particular interest is the porosity noted for these samples (Figure 9b). This is not believed to be due to a beam effect since the destruction of the wire was observed by longer beam exposure and could be reproducibly generated. Similarly, dots, tadpoles, and some wires were noted for **7** (Figure 9c); however, in contrast to **6** the components appear smooth. It is of note that no polymers were used in this ES process, and wire and wire-like materials were observed in several instances. Attempts to generate nanowires for the other systems involved several adjustments including varying the precursor concentrations of the other solutions. Unfortunately, this did not lead to the desired sample morphology.

PXRD of a sample isolated after prolonged ES processing indicated that an amorphous powder was isolated. FTIR data revealed the presence of carboxylate moieties, which indicates the isolated wires consist of cross-linked metalorganic species or the MO_x core is protected by ORc groups. Either description indicates that the wires noted are *not* the fully crystalline oxide materials of interest, and careful thermal processing should allow for conversion to an oxide wire.

■ SUMMARY AND CONCLUSION

A series of carboxylate group 4 species were crystallographically characterized as a mono- (**1** and **3**), di- (**4**−**7**), or tetranuclear (**2**) species. Compounds **4**−**7** are the first homoleptic carboxylic acid derivatives reported. NMR data indicated a great deal of dynamic ligand behavior occurs for these compounds upon dissolution. Both PFG NMR diffusion and elemental analyses confirmed the purity of the bulk powders with only one species noted in solution (THF-d_8) for **2**−**7** (minor species noted for **1** and **1b**). ES of these compounds with no added polymer led to direct formation of wire-like species for **4** and **6** and wires for **7**. Melting point determinations indicated that the stability of the compounds followed the general cation progression Ti < Hf < Zr, which correlated with the intermediate species forming wires. Additional work is under way to determine and exploit the driver/controlling aspect of these compounds and other metal

systems to directly ES wires; however, the current system appears to be fine-tuned for the ES of wires by **7**. Given the many variables available in ES (i.e., collector distance, voltage, concentration, etc.), optimization of wire formation should be available for this novel family of compounds, but additional studies are necessary to pinpoint the controlling properties.

■ ASSOCIATED CONTENT

Supporting Information

Listings of experimental data and structural information for **1a**, additional structure plots of **2** and **6a**, TGA data for **1**−**7**, and additional SEM data for **1**−**7**. This material is available free of charge via the Internet at http://pubs.acs.org. CCDC 983520−983528 contain the supplementary crystallographic data for **1**−**7**, respectively. These data can be obtained free of charge via http://www.ccdc.cam.ac.uk/conts/retrieving.html or from the Cambridge Crystallographic Data Centre, 12 Union Road, Cambridge CB2 1EZ, UK; fax: (+44) 1223-336-033; or e-mail: support@ccdc.cam.ac.uk.

■ AUTHOR INFORMATION

Corresponding Author

*E-mail tjboyle@sandia.gov. Phone: (505)272-7625. Fax: (505)272-7336.

Notes

The authors declare no competing financial interest.

■ ACKNOWLEDGMENTS

For support of this research, the authors thank Dr. N. S. Bell for assistance with the viscosity measurements and the Laboratory Directed Research and Development (LDRD) program at Sandia National Laboratories and the U.S. Department of Energy, Office of Electricity, under Contract DE-AC04-94AL85000. Sandia is a multiprogramming laboratory operated by Sandia Corporation, a Lockheed Martin Company, for the United States Department of Energy.

■ REFERENCES

(1) Boch, P.; Niepce, J.-C. *Ceramic Materials: Processes, Properties, and Applications*; ISTE Ltd.: Newport Beach, CA, 2007.
(2) Pomogailo, A. D.; Dzhardimalieva, G. I.; Kestelman, V. N. *Macromolecular Metal Carboxylates and Their Nanocomposites*; Springer: Berlin, 2010; Vol. *X*, p 306.
(3) Mehrotra, R. C.; Bohra, R. *Metal Carboxylates*; Academic Press: New York, 1983; p 396.
(4) *Conquest* Version 1.16; Cambridge Crystallographic Data Centre: support@ccdc.cam.ac.uk or http://www.ccdc.cam.ac.uk [CSD version 5.35 (November 2013)].
(5) Gross, S.; Kickelbick, G.; Puchberger, M.; Schubert, U. *Monatsh. Chem.* **2003**, *134*, 1053−1063.
(6) Kickelbick, G.; Schubert, U. *Chem. Ber.* **1997**, *130*, 473−477.
(7) Kickelbick, G.; Schubert, U. *Eur. J. Inorg. Chem.* **1998**, 159−161.
(8) Trimmel, G.; Gross, S.; Kickelbick, G.; Schubert, U. *Appl. Organomet. Chem.* **2001**, *15*, 401−406.
(9) Walther, P.; Puchberger, M.; Kogler, F. R.; Schwarz, K.; Schubert, U. *Phys. Chem. Chem. Phys.* **2009**, *11*, 3640−3647.
(10) Frot, T.; Cochet, S.; Laurent, G.; Sassoye, C.; Popall, M.; Sanchez, C.; Rozes, L. *Eur. J. Inorg. Chem.* **2010**, 5650−5659.
(11) Piszczek, P.; Richert, M.; Grodzicki, A.; Glowiak, T.; Wojtczak, A. *Polyhedron* **2005**, *24*, 663−670.
(12) Schaate, A.; Roy, P.; Godt, A.; Lippke, J.; Waltz, F.; Wiebcke, M.; Behrens, P. *Chem.—Eur. J.* **2011**, *17*, 6643−6651.
(13) Chaumont, C.; Huen, E.; Huguenard, C.; Mobian, P.; Henry, M. *Polyhedron* **2013**, *57*, 70−76.
(14) Petit, S.; Morlens, S.; Zeming, Y.; Luneau, D.; Pilet, G.; Soubeyroux, J.-L.; Odier, P. *Solid State Sci.* **2011**, *13*, 665−670.
(15) Tararam, R.; Foschini, C. R.; Destro, F. B.; Simoes, A. Z.; Longo, E.; Varela, J. A. *J. Alloys Cmpds.* **2014**, *604*, 175−180.
(16) Zhao, Y.; Jiang, P. *Colloids Surf. A* **2014**, *444*, 232−239.
(17) Zhang, Q.; Nakamoto, T.; Chen, S. W.; Kawazoe, N.; Lin, K. L.; chang, J.; Chen, G. P. *J. Nanosci. Nanotechnol.* **2014**, *14*, 3221−3227.
(18) Knag, P. G.; Yun, B. K.; Sung, K. D.; Lee, T. K.; Lee, M.; Lee, N.; Oh, S. H.; Jo, W.; Seog, H. J.; Ahn, C. W.; Kim, I. W.; Jung, J. H. *RSC Adv.* **2014**, *4*, 29799−29805.
(19) Wen, T. A.; Pingguan-Murphy, B.; Ahmad, R.; Akbar, S. A. *J. Mater. Sci.* **2013**, *48*, 8337−8353.
(20) Burger, C.; Hsiao, B. S.; Chu, B. *Annu. Rev. Mater. Res.* **2006**, *36*, 333−368.
(21) Greiner, A.; Wendorff, J. H. *Angew. Chem., Int. Ed.* **2007**, *46*, 5670−5703.
(22) Ramakrishna, S. *An Introduction to Electrospinning and Nanofibers*; World Scientific: Singapore; Hackensack, NJ, 2005; p 382.
(23) Reneker, D. H.; Yarin, A. L. *Polymer* **2008**, *49*, 2387−2425.
(24) Dersch, R.; Graeser, M.; Greiner, A.; Wendorff, J. H. *Aust. J. Chem.* **2007**, *60*, 719−728.
(25) Boyle, T. J.; Doan, T. Q.; Steele, L. M.; Hoppe, S. M.; Hawthorne, K.; Kalinich, R. M.; Sigmund, W. M. *Dalton Trans* **2012**, *41*, 9349−9364.
(26) Boyle, T. J.; Steele, L. A.; Burton, P. D.; Hoppe, S.; Lockhart, C.; Rodriguez, M. A. *Inorg. Chem.* **2012**, *51*, 12075−12092.
(27) Boyle, T. J.; Tyner, R. P.; Alam, T. M.; Scott, B. L.; Ziller, J. W.; Potter, B. G. *J. Am. Chem. Soc.* **1999**, *121*, 12104−12112.
(28) Callaghan, P. T. *Principles of Nuclear Resonance Microscopy*; Oxford University Press: Oxford, 1991; p 492.
(29) Moraru, B.; Gross, S.; Kickelbick, G.; Trimmel, G.; Schubert, U. *Monatsh. Chem.* **2001**, *132*, 993−999.
(30) Pajot, N.; Papiernik, R.; Hubert-Pfalzgraf, L. G.; Vaissermann, J.; Parraud, S. *Chem. Commun.* **1995**, 1817−1819.
(31) Benedict, J. B.; Coppens, P. *J. Am. Chem. Soc.* **2010**, *132*, 2938.
(32) Forte, C.; Hayatifar, M.; Pampaloni, G.; Galletti, A. M. R.; Fenili, F.; Zacchini, S. *J. Polym. Sci., Part A: Polym. Chem.* **2011**, *49*, 3338−3345.
(33) Straessler, N. A.; Caudle, M. T.; Groy, T. L. *Acta Crystallogr., Sect. E: Struct. Rep. Online* **2008**, *E64*, m48−U502.
(34) Dell'Amico, D. B.; Calderazzo, F.; Lanelli, S.; Labella, L.; Marchetti, F.; Pelizzi, G. *J. Chem. Soc., Dalton Trans.* **2000**, 4339−4342.
(35) Campana, C. F.; Chen, Y.; Day, V. W.; Kemperer, W. G.; Sparks, R. A. *J. Chem. Soc., Dalton Trans.* **1996**, 691−702.
(36) Berger, E.; Westin, G. *J. Sol-Gel Sci. Technol.* **2010**, *53*, 681−688.
(37) Shannon, R. D. *Acta Crystallogr.* **1976**, *A32*, 751−767.
(38) Puchberger, M.; Kogler, F. R.; Jupa, M.; Gross, S.; Fric, H.; Kickelbick, G.; Shubert, U. *Eur. J. Chem.* **2006**, 3283−3293.
(39) Evans, W. J.; Nyce, G. W.; Greci, M. A.; Ziller, J. W. *Inorg. Chem.* **2001**, *40*, 6725−6730.